

Gradiometry for polarized seismic waves

Charles A. Langston¹ and Chuntao Liang¹

Received 6 November 2007; revised 16 May 2008; accepted 30 May 2008; published 1 August 2008.

[1] Wave gradiometry for a generic point source wave model in cylindrical coordinates is developed to utilize the horizontal components of seismic wavefields. Attributes of *P-SV* and *SH* waves such as horizontal slowness and its change, the change in geometrical spreading, the change in radiation pattern, azimuth of propagation, and wave polarization can be determined by measuring the horizontal strains and rotations of the wavefield along with three components of displacement. Gradiometer cells composed of an array of three-component seismographs can be used to provide estimates of the wave gradients. Alternatively, a single three-component seismograph collocated with an areal strainmeter (for *P-SV* waves) or a rotation sensor (for *SH* waves) can be used to estimate wave polarization and the slowness/amplitude behavior of one aspect of the wavefield. Wave gradients are computed for the 1 April 2007 Solomon Island earthquake using data from the ANZA Seismic Network in southern California and show excellent consistency among stations of the network. Azimuth and slowness of various long-period teleseismic waves are recovered using gradiometry analysis. The consistency of strains computed from the broadband array suggests that they may be used to calibrate Plate Boundary Observatory tensor strainmeters in the region.

Citation: Langston, C. A., and C. Liang (2008), Gradiometry for polarized seismic waves, *J. Geophys. Res.*, *113*, B08305, doi:10.1029/2007JB005486.

1. Introduction

[2] The density and high quality of seismic station installations are reaching a point where areal changes in observed seismic wavefields can be used to infer fundamental wave propagation characteristics independent of knowledge of the Earth structure. The physical basis of this kind of seismometry is actually the physical basis of elastodynamics through the relationship of stress, strain, and resulting equations of motion. Dense arrays of seismometers can be utilized to estimate “geodetic” strains and rotations induced by a seismic event over a region of the Earth through numerical spatial derivatives of the observed wavefield [Bodin *et al.*, 1997; Gomberg *et al.*, 1999; Spudich *et al.*, 1995; Igel *et al.*, 2005]. Seismic strains and rotations are fundamentally different wavefield observables from ground displacements or velocities and contain rich information about the nature of the seismic waves that can be used to identify wave type, directions of propagation, phase speeds, and amplitude variations with distance and azimuth [Langston, 2007a, 2007b, 2007c]. Indeed, it is starting to become possible to study the full characterization of the wave dynamics of a point in the Earth using the full 6 degrees of freedom of displacement and rotation motion [Nigbor, 1994].

[3] A previous set of papers outlined a method termed “wave gradiometry” that incorporated simple models of a propagating scalar seismic or acoustic wave to utilize wave

spatial gradients and velocities to determine wave attributes [Langston, 2007a, 2007b, 2007c]. The spatial gradient of displacement over 1-D and 2-D surface arrays of seismometers can be linearly related to the velocity and displacement time series at a point using an assumption of a propagating wave with distance-dependent geometrical spreading. Solving for the coefficients of this linear relationship yields useful wave parameters such as horizontal slowness, changes in geometrical spreading, changes in radiation pattern, and wave propagation azimuth.

[4] In this paper we extend wave gradiometry to utilize three components of vector ground motion in addition to horizontal strains and rotations. This generalization of the method yields several interesting practical results that integrate observation programs in broadband seismometry, strainmeter instrumentation [Agnew, 1986; Gladwin, 2007; Roeloffs *et al.*, 2004; University NAVSTAR Consortium (UNAVCO), 2004], and rotation meter instrumentation [Cochard *et al.*, 2006; Igel *et al.*, 2005; Suryanto *et al.*, 2006; Takeo and Ito, 1997]. In particular, we find several simple relationships between the spatial gradients of a propagating wave radiated from a point source that yield estimates of wave azimuth in addition to results from the previous wave gradiometry technique. We also find relationships between the areal strain and ground motions for *P-SV* waves and rotation about the vertical with ground motions from *SH* waves that use similar gradiometry equations. Theoretical results suggest the possibility of several kinds of “point” seismic arrays that could be constructed and used to analyze wavefields. From a practical standpoint, we also show that it is possible to derive a strain and rotation field from an array of seismometers that

¹Center for Earthquake Research and Information, University of Memphis, Memphis, Tennessee, USA.

is self-consistent for a region that might be used as a reference strain field to calibrate existing borehole tensor strainmeters. This is shown using data from the ANZA Seismic Network in southern California. We also suggest that three-component wave gradiometry can be usefully applied to existing large seismic arrays to determine how wave attributes change with geographic position for use in large-scale Earth structure studies.

2. Determining Wave Azimuth From Horizontal Gradients

[5] The main problem is to find a relationship between seismic wave horizontal gradients in the cylindrical coordinate system for a point source and the geocentric, Cartesian coordinate system used for seismic observation. The difficulty is that *P-SV* and *SH* waves are generally mixed and interfere with each other on horizontal components of ground motion in the usual geocentric (N-S/E-W) coordinate system if source location is not known. Thus, the determination of wave propagation azimuth is the principal problem to be solved in unraveling the polarization of incident seismic waves from observed Cartesian displacement gradients. Once azimuth is known, it becomes straightforward to apply all of the previous results obtained for scalar waves in 2-D wave gradiometry. In the following, Langston [2007a, 2007b, 2007c] will be referred to as papers 1, 2, and 3.

[6] We assume a cylindrical wave model based on the form of propagating wave solutions of a point source in vertically heterogeneous media [e.g., Helmberger, 1983]. These kinds of wave equation solutions are commonly used in modeling observed seismograms at local, regional, and teleseismic distance in all but the lowest-frequency bands. In general, our ansatz, or assumed solution for the wave function, is just a little more complicated than a plane wave model since it includes the effects of geometrical spreading and radiation pattern. This is done so that the theory can be used for arrays of instruments close to a seismic source such as in regional or local seismometry. Depending on source distance, the equations may lead to simplifications where plane waves or cylindrical waves without azimuthal amplitude changes may be appropriate to model the wavefield. In the following, we also assume explicit forms of the cylindrical and Cartesian wave function to knit together the development of gradiometry from papers 1–3. Assuming a point source at some depth under the origin of the coordinate system of Figure 1, further assume that the vertical, u_z , radial, u_r , and transverse, u_θ , displacements are given by

$$\begin{aligned} u_z &= G_R(r)R_R(\theta)f_z[t - p_R(r)(r - r_0)], \\ u_r &= G_R(r)R_R(\theta)f_r[t - p_R(r)(r - r_0)], \\ u_\theta &= G_L(r)R_L(\theta)f_\theta[t - p_L(r)(r - r_0)], \end{aligned} \quad (1)$$

where the *P-SV* (or “Rayleigh wave”) geometrical spreading and source radiation pattern are $G_R(r)$ and $R_R(\theta)$, respectively, and the *SH* (or “Love wave”) corresponding functions are $G_L(r)$ and $R_L(\theta)$. Also note that the horizontal slownesses, p_R and p_L , are functions of r . The time history of each wave can be different, but the *P-SV* system horizontal slowness, p_R , is the same between vertical and

radial components. The *SH* horizontal slowness, p_L , is generally different than the *P-SV* slowness. Equations (1) describe the far-field propagation of a single *P-SV* wave and a single *SH* wave and are not appropriate for waves in the near field of a seismic source. This wave ansatz will be used in a similar way as in papers 1 and 2 in that we will assume that a seismogram will be composed of only one wave within any particular time interval except where *P-SV* and *SH* motions mix on horizontal components since

$$\begin{aligned} u_1 &= u_r \sin \theta + u_\theta \cos \theta \\ u_2 &= u_r \cos \theta - u_\theta \sin \theta. \end{aligned} \quad (2)$$

[7] If the azimuth, θ , is known from source location, then the radial and azimuthal spatial gradients of the waves in equations (1) can be simply derived using the chain rule of differential calculus to obtain

$$\begin{bmatrix} u_{z,r} \\ \frac{u_{z,\theta}}{r} \\ u_{r,r} \\ \frac{u_{r,\theta}}{r} \\ u_{\theta,r} \\ \frac{u_{\theta,\theta}}{r} \end{bmatrix} = \begin{bmatrix} A_R & B_R & 0 & 0 & 0 & 0 \\ \frac{\Re_R}{r} & 0 & 0 & 0 & 0 & 0 \\ 0 & 0 & A_R & B_R & 0 & 0 \\ 0 & 0 & \frac{\Re_R}{r} & 0 & 0 & 0 \\ 0 & 0 & 0 & 0 & A_L & B_L \\ 0 & 0 & 0 & 0 & \frac{\Re_L}{r} & 0 \end{bmatrix} \begin{bmatrix} u_z \\ \dot{u}_z \\ u_r \\ \dot{u}_r \\ u_\theta \\ \dot{u}_\theta \end{bmatrix}, \quad (3)$$

where the overdot denotes time differentiation and the comma denotes spatial differentiation with respect to a cylindrical coordinate. The coefficients in the square matrix are

$$\begin{aligned} A_R &= \frac{G'_R}{G_R}, \\ A_L &= \frac{G'_L}{G_L}, \end{aligned} \quad (4)$$

$$\begin{aligned} B_R &= -p_R - \frac{\partial p_R}{\partial r}(r - r_0), \\ B_L &= -p_L - \frac{\partial p_L}{\partial r}(r - r_0), \end{aligned} \quad (5)$$

and

$$\begin{aligned} \Re_R(\theta) &= \frac{R'_R}{R_R}, \\ \Re_L(\theta) &= \frac{R'_L}{R_L}. \end{aligned} \quad (6)$$

The prime denotes the derivative with respect to the function argument.

[8] Basically, equations (3) say that the radial gradient in displacement is proportional to the velocity, scaled by horizontal wave slowness, and the displacement, scaled by the geometrical spreading. The azimuth derivatives in

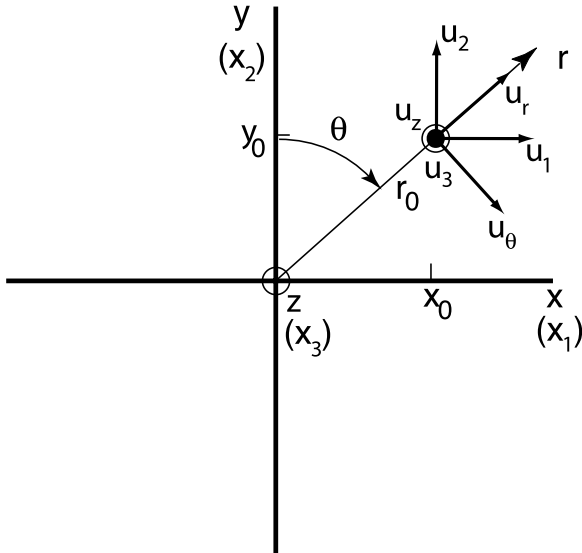


Figure 1. Coordinate conventions for the Cartesian and cylindrical coordinate systems used in this paper. In addition, x and y directions correspond to east and north geographic directions.

equations (3) are proportional to the displacement. Horizontal wave slowness, changes in geometrical spreading, changes in radiation pattern, and source azimuth can be derived from these relationships using the results for the vertical component of motion addressed in paper 2. The radial and azimuthal coefficients (equations (4), (5), and (6)) were found by writing the displacement for the cylindrical wave in terms of Cartesian displacements and solving two 1-D problems for the corresponding Cartesian coefficients in x and y .

[9] It is useful to see how the cylindrical wave coefficients are related to the Cartesian coefficients to tie the theory together for scalar and polarized waves propagating in two dimensions. The Cartesian formulation is the basis for initial processing of data. Cylindrical wave attributes are derived from these Cartesian coefficients. Ignoring near-field terms like u_r/r , the cylindrical derivatives are related to Cartesian derivatives in the geographical coordinate system (Figure 1) by

$$\begin{bmatrix} u_{z,r} \\ \frac{u_{z,\theta}}{r} \\ u_{r,r} \\ \frac{u_{r,\theta}}{r} \\ u_{\theta,r} \\ \frac{u_{\theta,\theta}}{r} \end{bmatrix} = \begin{bmatrix} \mathbf{V} & 0 \\ 0 & \mathbf{U} \end{bmatrix} \begin{bmatrix} u_{3,1} \\ u_{3,2} \\ u_{1,1} \\ u_{1,2} \\ u_{2,1} \\ u_{2,2} \end{bmatrix}, \quad (7)$$

where

$$\mathbf{V} = \begin{bmatrix} \sin \theta & \cos \theta \\ \cos \theta & -\sin \theta \end{bmatrix} \quad (8)$$

and

$$\mathbf{U} = \begin{bmatrix} \sin^2 \theta & \cos \theta \sin \theta & \cos \theta \sin \theta & \cos^2 \theta \\ \cos \theta \sin \theta & -\sin^2 \theta & \cos^2 \theta & -\cos \theta \sin \theta \\ \cos \theta \sin \theta & \cos^2 \theta & -\sin^2 \theta & -\cos \theta \sin \theta \\ \cos^2 \theta & -\cos \theta \sin \theta & -\cos \theta \sin \theta & \sin^2 \theta \end{bmatrix}. \quad (9)$$

Matrices \mathbf{V} and \mathbf{U} are unitary matrices where $\mathbf{V} = \mathbf{V}^T = \mathbf{V}^{-1}$ and $\mathbf{U} = \mathbf{U}^T = \mathbf{U}^{-1}$.

[10] Azimuth, θ , must be known so that the cylindrical derivatives can be derived from the Cartesian derivatives that occur on the right-hand side of equation (7). For example, following the results of paper 2, the equivalent form of the vertical component of displacement in Cartesian coordinates is

$$u_3 = G(x, y) f [t - p_x(x - x_0) - p_y(y - y_0)]. \quad (10)$$

Note that the Cartesian spatial function G takes up both the radiation pattern and the geometrical spreading of the wave. Paper 2 shows in detail how the individual x and y displacement gradients on the right-hand side of equation (7) can be treated in separate 1-D gradiometry problems to obtain horizontal wave slowness and geometrical spreading changes in their respective directions. Both quantities are then related to the radial and azimuthal coefficients of equations (4), (5), and (6). In particular,

$$\begin{aligned} A_R &= A_x \sin \theta + A_y \cos \theta, \\ B_R &= B_x \sin \theta + B_y \cos \theta, \end{aligned} \quad (11)$$

and

$$\begin{aligned} A_x &= A_R \sin \theta, \\ A_y &= A_R \cos \theta, \\ B_x &= B_R \sin \theta, \\ B_y &= B_R \cos \theta, \end{aligned} \quad (12)$$

where

$$\begin{aligned} u_{3,1} &= A_x u_3 + B_x \dot{u}_3, \\ u_{3,2} &= A_y u_3 + B_y \dot{u}_3. \end{aligned} \quad (13)$$

Substitution of the cylindrical coefficients in equation (12) into equation (13) gives the first new result where

$$\tan \theta = \frac{u_{3,1}}{u_{3,2}}. \quad (14)$$

This states that the wave propagation azimuth can be found from the Cartesian spatial gradients of the vertical component of motion without recourse to any detailed gradiometry analysis for slowness or geometrical spreading as presented in paper 2. This is a significant simplification for finding wave azimuth and is independent of any possible radiation pattern that the source might have.

[11] However, what happens to the gradiometry problem when the azimuth is not known from a source and horizontal ground motion components or gradients are available? In this case the displacements and displacement gradients are

mixed through equation (2). Ignoring near-field derivatives, the relationships between the cylindrical and Cartesian gradients are

$$\mathbf{b} = \mathbf{Ud}, \quad \mathbf{d} = \mathbf{Ub}, \quad (15)$$

where

$$\mathbf{b} = \begin{bmatrix} u_{r,r} \\ u_{r,\theta} \\ r \\ u_{\theta,r} \\ \frac{u_{\theta,\theta}}{r} \end{bmatrix} \quad (16)$$

and

$$\mathbf{d} = \begin{bmatrix} u_{1,1} \\ u_{1,2} \\ u_{2,1} \\ u_{2,2} \end{bmatrix}. \quad (17)$$

[12] If an event is close enough in distance, then radiation pattern terms may be large enough to produce coupling between u_r and u_θ derivatives through equations (15). In other words, the Cartesian derivatives are functions of both *P-SV* and *SH* wavefield gradients. For teleseismic or regional events at great distance, radiation pattern changes across a small gradiometer cell will be much smaller than the radial changes that include wave slowness. In this case, an isotropic source assumption can be used to estimate azimuth by neglecting the azimuthal derivatives. Note that this is not the same as a plane wave assumption since radial geometrical spreading changes may still occur. The derivative relations simplify such that

$$\begin{bmatrix} u_{1,1} \\ u_{1,2} \\ u_{2,1} \\ u_{2,2} \end{bmatrix} = \mathbf{U} \begin{bmatrix} u_{r,r} \\ 0 \\ u_{\theta,r} \\ 0 \end{bmatrix}. \quad (18)$$

Taking the ratios of the Cartesian gradients gives the next two new results of

$$\tan \theta = \frac{u_{1,1}}{u_{1,2}} = \frac{u_{2,1}}{u_{2,2}}. \quad (19)$$

Equation (19) can also be derived quickly without considering simplifications of the matrix in equation (18) simply by considering that the *SV* and *SH* waves that make up the horizontal displacements are purely functions of distance, r . However, the analogous equation for the vertical component of motion (equation (14)) was derived without the simplification of an isotropic point source; that is, a radiation pattern may be present. Thus, we get a set of remarkably simple relationships for obtaining wave azimuth from the ratios of horizontal Cartesian displacement gradients in all three components. Equations (14) and (19) can be applied directly to the spatial gradients of the seismic

displacement field without determining wave slownesses or geometrical spreading changes implicit in the previous wave gradiometry method of paper 2.

[13] Once azimuth is known, cylindrical displacement derivatives (equations (7)) can be computed using the value of azimuth and the Cartesian horizontal displacement gradients. Under this isotropic point source assumption, all of the cylindrical derivatives can be found from Cartesian derivatives, the seismic data can be rotated into the direction of the wave azimuth to obtain radial and transverse motions, and the wave parameters can be determined using the techniques of papers 2 and 3 and equations (3)–(6). One simplifying case of interest is for a plane wave where the radiation pattern, geometrical spreading coefficients, and horizontal slownesses are constant. Equation (3) then simplifies to

$$\begin{bmatrix} u_{z,r} \\ u_{r,r} \\ u_{\theta,r} \end{bmatrix} = \begin{bmatrix} -p_R & 0 & 0 \\ 0 & -p_R & 0 \\ 0 & 0 & -p_L \end{bmatrix} \begin{bmatrix} \dot{u}_z \\ \dot{u}_r \\ \dot{u}_\theta \end{bmatrix}. \quad (20)$$

3. Strain and Rotation

[14] The horizontal component displacement gradients are naturally related to both the dynamic strain and rotation of the seismic wavefield [Gomberg and Agnew, 1996; Gomberg et al., 1999; Igel et al., 2005]. Merging seismic, strain, and rotation measurements through wave gradiometry concepts offers a way to decouple these two horizontal wavefields and also brings up new ways of observing and understanding wave propagation in the Earth. It is of some interest to investigate what gradiometry quantities can be obtained from typical strain and rotation instruments.

[15] Long-baseline laser strainmeters [Agnew, 1986] and borehole Gladwin Tensor Strainmeters (GTSM) [Roeloffs et al., 2004; UNAVCO, 2004] measure three independent horizontal strains. Usually presented in the geocentric coordinate system, the two displacement gradients, $u_{1,1}$ and $u_{2,2}$, can be derived from the elongation in the E-W and N-S directions, respectively, but the other two horizontal displacement gradients, $u_{1,2}$ and $u_{2,1}$, that are needed for a wave azimuth determination under the isotropic source assumption (equation (19)) occur in linear combination as the shear strain, $\frac{1}{2}(u_{1,2} + u_{2,1})$. Thus, a strainmeter is only a partial horizontal gradiometer. On the other hand, there have been recent efforts in measurement of the horizontal rotation field using sensitive Sagnac laser interferometers [Cochard et al., 2006; Igel et al., 2005; Suryanto et al., 2006]. These interferometers measure rotation, -2ψ , around the vertical axis in which

$$\psi = -(\nabla \times \mathbf{u})_z = (u_{1,2} - u_{2,1}). \quad (21)$$

Combining the observations of a tensor strainmeter with that of a horizontal rotation meter would yield four independent measurements of strain and rotation that could be used to derive the four horizontal displacement gradients. The addition of observations from one three-component seismometer at the same point on the Earth would complete the instrumentation needed for a point gradiometer array

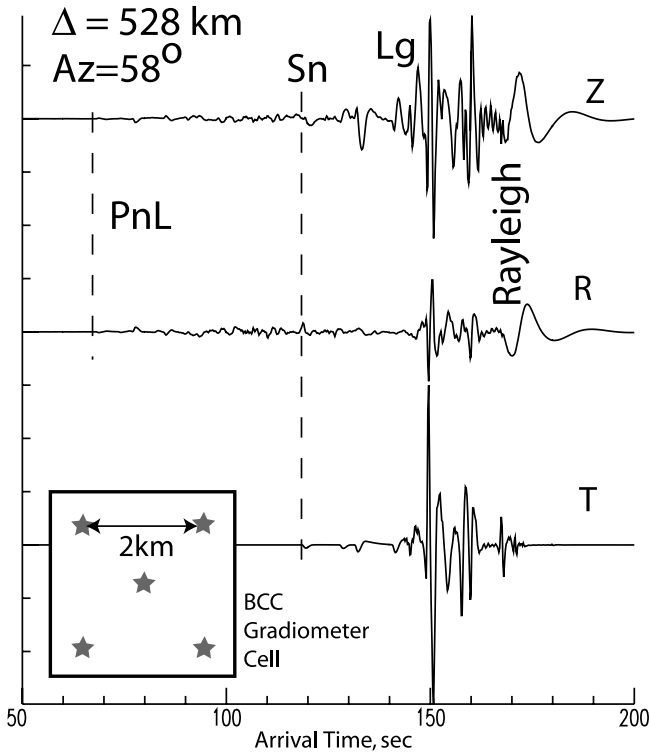


Figure 2. Broadband synthetic ground displacements for the center station of a small gradiometer cell 528 km from a point dislocation source. Shown are vertical (Z), radial (R), and transverse (T) ground motions. The wave propagation direction is 58°. The crustal model consists of a linear gradient crust over mantle half-space and all source and structure parameters as given by *Langston et al.* [2002]. The inset shows the geometry of a small array (“cell”) of receiver locations that is used to numerically compute the spatial derivatives of the ground displacements using the results of paper 2. The synthetic seismograms are computed using a full wavefield, wave number integration method and contain multiply reflected and refracted body waves in addition to surface waves. Sections of the seismograms are annotated to show the dominant wave types.

that could be used to infer all of the wavefield characteristics available through gradiometry analysis.

[16] Strain and rotation meters are each sensitive to different parts of the horizontal wavefield. It is straightforward to show from equations (15) and (3) that the horizontal rotation about the vertical axis is usually dominated by the SH portion of the cylindrical wavefield

$$\begin{aligned} \psi &= u_{1,2} - u_{2,1} = u_{\theta,r} + \frac{u_{\theta,\theta}}{r} = u_{\theta,r} + \Re_R \frac{u_r}{r} \\ &= A_L u_\theta + B_L i u_\theta + \Re_R \frac{u_r}{r} \end{aligned} \quad (22)$$

and that the area strain, φ , which is a strain invariant, is dominated by the P-SV wavefield

$$\begin{aligned} \varphi &= u_{1,1} + u_{2,2} = u_{r,r} - \frac{u_{\theta,\theta}}{r} = u_{r,r} - \Re_L \frac{u_\theta}{r} \\ &= A_R u_r + B_R i u_r - \Re_L \frac{u_\theta}{r}. \end{aligned} \quad (23)$$

Suryanto et al. [2006] used the plane wave approximation of equation (22) ($A_L = 0$, $\Re_R = 0$) to show how rotation computed for a teleseism from an irregular array of broadband stations had excellent agreement with the signal from a collocated Sagnac interferometer. *Gomberg and Agnew* [1996] estimated plane wave, surface wave strains from broadband seismograph observations, and knowledge of phase velocity dispersion in southern California to compare them with strains recorded by the long-baseline laser strainmeter at Pinon Flat Observatory. They found occasional large signals in the observed azimuthal strain that were unexpected and attributed to the effects of lateral heterogeneity.

[17] Under the isotropic source assumption ($\Re_L = \Re_R = 0$) and where azimuth is known for an event, an installation containing a single strainmeter and a three-component seismic instrument would be able to estimate wave slowness and geometrical spreading changes for the P-SV wavefield. Under the same assumptions, a single horizontal rotation meter and a collocated three-component seismic instrument would allow analysis of similar wavefield parameters for SH-type motion. An installation comprising a strainmeter and a horizontal rotation meter would be able to estimate source azimuth directly through use of equation (19). Wave parameters could be obtained using observations from an additional three-component seismic instrument. These are examples of a new concept that could be called the point seismic array [*Aldridge et al.*, 2006] since strain, rotation, and velocity measurements at a single location on the Earth would yield information about the wavefield that, in the past, has been the domain of extensive phased arrays of individual seismometers.

4. A Synthetic Seismogram Example

[18] The results of *Suryanto et al.* [2006] suggest that highly calibrated arrays of seismographs can be used to estimate accurate displacement gradients for long-period waves. Here we demonstrate some of the wave gradiometry concepts presented in this paper with a synthetic regional seismogram computation for a point source in vertically inhomogeneous media.

[19] Figure 2 displays synthetic broadband seismograms computed for a linear gradient crustal model over an isotropic half-space mantle. The Earth model and earthquake point source parameters are taken from *Langston et al.* [2002], who modeled regional waveform data within Tanzania, East Africa, using the “phase-time” inversion technique to obtain a crust and upper mantle model that explained the arrival times and amplitudes of most regional phases on the three-component seismograms. Details of the computation are given by Langston et al. The important aspect of these synthetic seismograms is that they contain numerous, interfering P, SV, and SH waves that refract, reflect, and occur as surface waves in each component. The application of wave gradiometry is based on a simple assumption of a single propagating wave in any one time interval on the seismogram. Papers 1 and 2 discuss the problems of interfering waves and how the basic assumption may be violated. This synthetic seismogram example displays how azimuth and wave parameter estimates can be robust where the wave propagation may be complex.

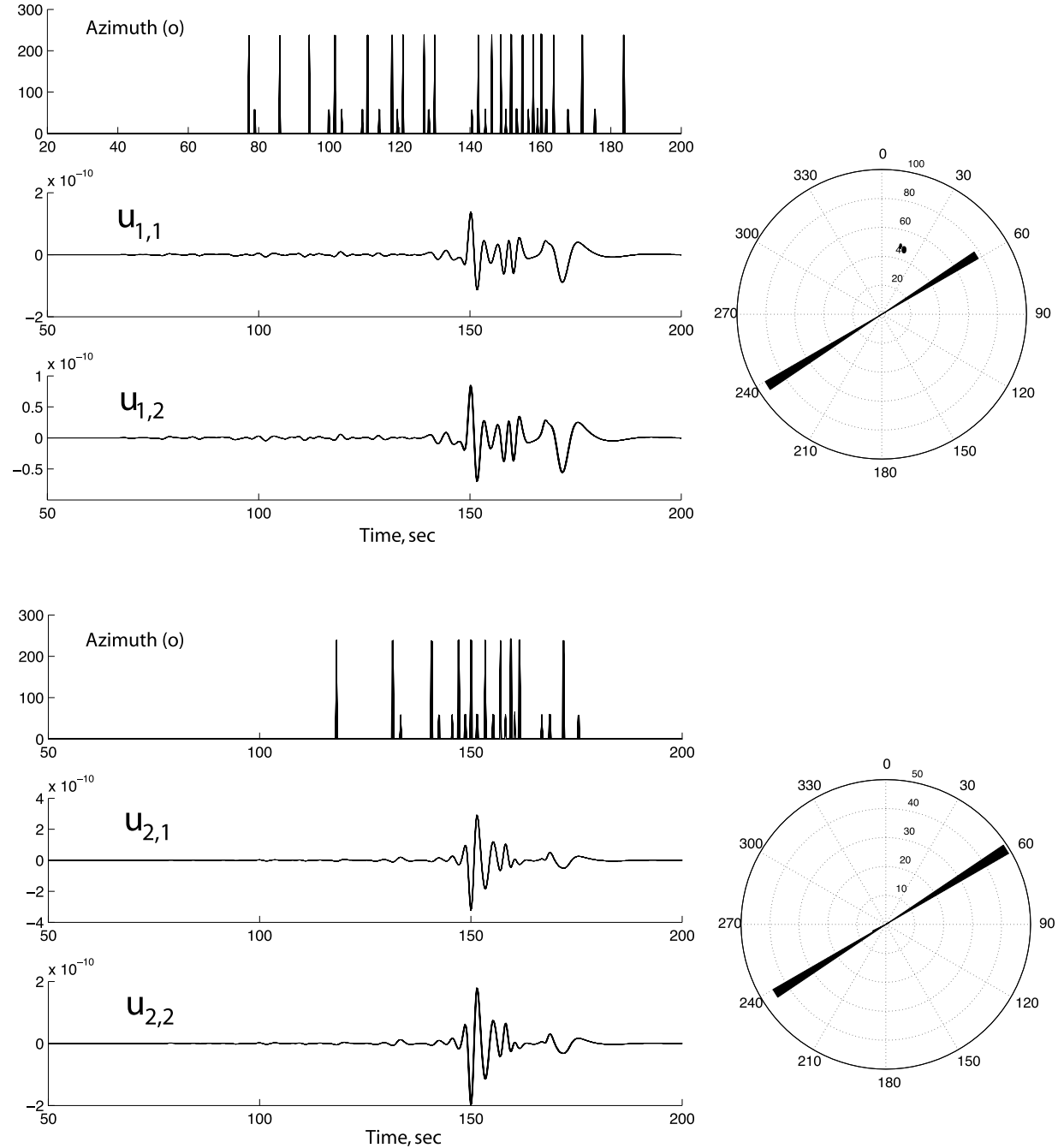


Figure 3. Azimuth analysis of the synthetic horizontal ground motions using equation (20). Shown are the horizontal derivatives of the horizontal ground motions. Wave azimuth is computed using the peaks and troughs of the wave gradients that are larger than 2% of the total ground motion. The horizontal motions contain both P - SV and SH wave types. The expected theoretical azimuth is resolved to 0.5° .

[20] A synthetic array of stations in body-centered cubic geometry (Figure 2) was assumed to enable the computation of the displacement gradients using the finite difference technique of paper 2. The data were band-pass filtered between 0.01 and 0.3 Hz using a two-pole phaseless Butterworth filter, and then the horizontal displacement gradients were computed. Figure 3 shows the result of applying equation (19) to determine source azimuth. To avoid zero amplitudes at zero crossings of the seismo-

grams, azimuth was only computed where a peak or trough was more than 2% of the maximum amplitude of the horizontal components. Although there is an ambiguity of 180° in the azimuth calculation, all estimated azimuths were within 0.5° of the true azimuth, mostly a testament to the numerical accuracy of the wave number integration program used to compute the synthetics and the recursive filter used to filter them. Note that the synthetic ground motions contained a mixture of P - SV and SH waves and

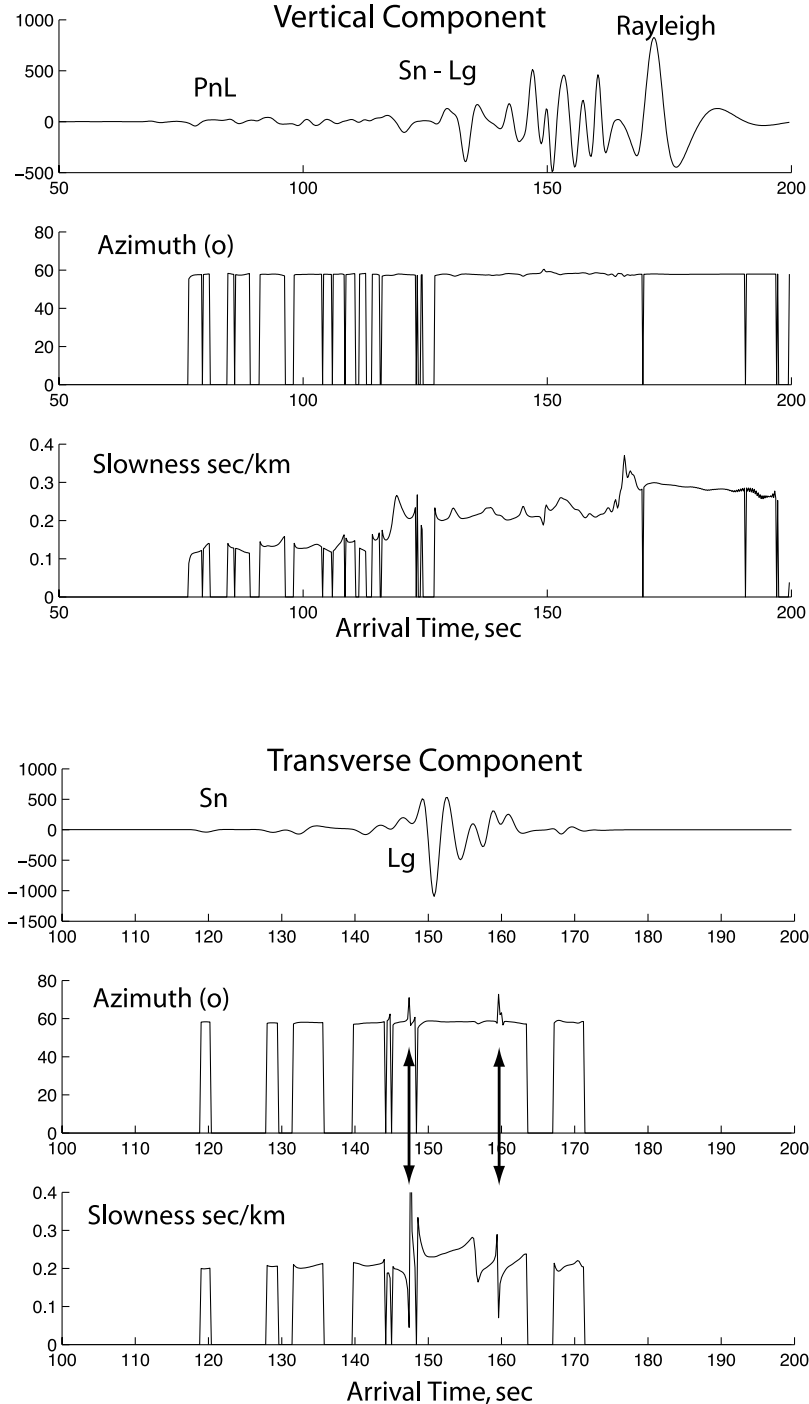


Figure 4. The 2-D gradiometry analysis of the (top) vertical and (bottom) transverse synthetic motions using the results of papers 2 and 3 in addition to equations (3)–(7). The arrows in Figure 4 (bottom) illustrate the kinds of artifacts that occur when two or more waves interfere with each other and are analyzed using the time domain method of paper 3. Otherwise, azimuth estimates are within 0.5° , and the slowness estimates are consistent with the type of body wave or surface wave contained within the seismograms.

that the azimuth computation used the isotropic source assumption.

[21] The 180° azimuth ambiguity is removed immediately either using a gradiometry analysis of the vertical component (Figure 4) or simply assuming one of the azimuth

directions to compute radial and transverse motions from the N-S and E-W motions. Although the assumed radial and transverse polarities may be incorrect, gradiometry will correctly identify the direction of wave propagation and

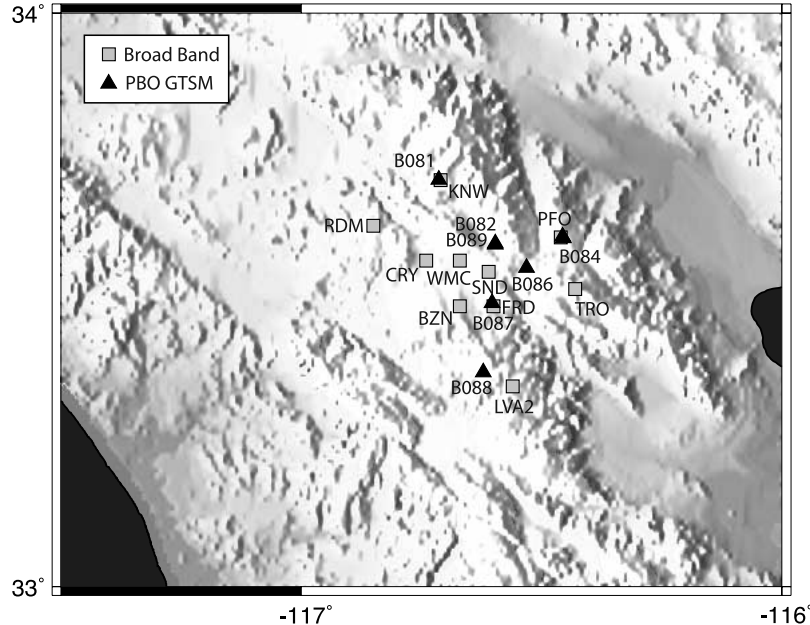


Figure 5. Index map of southern California showing the location of ANZA Seismic Network and collocated PBO GTSM stations.

its speed since the finite difference computation relies on phase differences for this information.

5. ANZA Seismic Network as a Gradiometer

[22] It is useful to demonstrate that horizontal gradiometry concepts work with real data sets. Nearly anything can go wrong with actual seismic data including problems with instrument installation and responses, the effects of lateral velocity heterogeneity, and superimposed ground motion noise fields. Unfortunately, there are few dense seismic arrays that can be used as a wave gradiometer. However, the ANZA Seismic Network, operated by University of California San Diego in southern California (Figure 5), is one such network that can be used as a long-period gradiometer for large teleseismic earthquakes. Part of the ANZA Seismic Network includes 10 stations dispersed within a 50 km diameter area. Instrumentation consists of Streckeisen STS-2 seismometers with Reftek 24-bit digitizers. Station spacing is roughly 10 km, which would potentially allow for the computation of accurate displacement gradients for 100 km wavelength waves (papers 1 and 2). This translates into wave periods of 25 s for a horizontal phase velocity of 4 km/s. In addition, the ANZA Seismic Network contains a network of Plate Boundary Observatory (PBO) GTSMs where seismically derived strains can be compared to individual GTSM strains.

[23] Seismic and GTSM strain data were collected for the 1 April 2007 $M8.1$ Solomon Islands earthquake from the Incorporated Research Institutions for Seismology and UNAVCO data centers. The 40 Hz sample rate broadband seismic data were corrected to ground displacement using the individual component instrument responses for the stations shown on Figure 5 [Goldstein *et al.*, 2003]. A

trapezoidal band-pass filter was assumed in the instrument response correction that had cutoff frequencies of 0.005 to 0.5 Hz with a central passband of 0.01 to 0.4 Hz and the data decimated to 10 Hz. Examination of the spectra in the frequency domain shows that all ground motion components have relatively flat spectra from 0.005 to 0.05 Hz with an order of magnitude falloff in amplitude after 0.05 Hz. Thus, no additional filtering was necessary. Figure 6 shows the horizontal component velocity data for all 10 stations with major teleseismic arrivals annotated. The event occurred at 91.7° distance from station FRD with a theoretical back azimuth along the great circle path of 261° . Note the remarkable consistency of all horizontal waveforms. Aside from some long-period background noise seen before major S arrivals, the waveform shapes and amplitudes are nearly identical between seismic stations.

[24] Displacement gradients were computed for this array at each station by using a variation of the method suggested by Spudich *et al.* [1995]. We did not make any assumptions on the nature of the vertical displacement gradients but simply examined the horizontal displacement gradients separately for each component. Station locations were referenced to station FRD as an origin. The horizontal displacement gradient is obtained for each time point by expanding the displacement in a Taylor's series about the location of a particular station at (x_0, y_0) :

$$\begin{aligned} u(x_1, y_1) &= u(x_0, y_0) + \left. \frac{\partial u}{\partial x} \right|_{x_0} (x_1 - x_0) + \left. \frac{\partial u}{\partial y} \right|_{y_0} (y_1 - y_0) \\ u(x_2, y_2) &= u(x_0, y_0) + \left. \frac{\partial u}{\partial x} \right|_{x_0} (x_2 - x_0) + \left. \frac{\partial u}{\partial y} \right|_{y_0} (y_2 - y_0). \end{aligned} \quad (24)$$

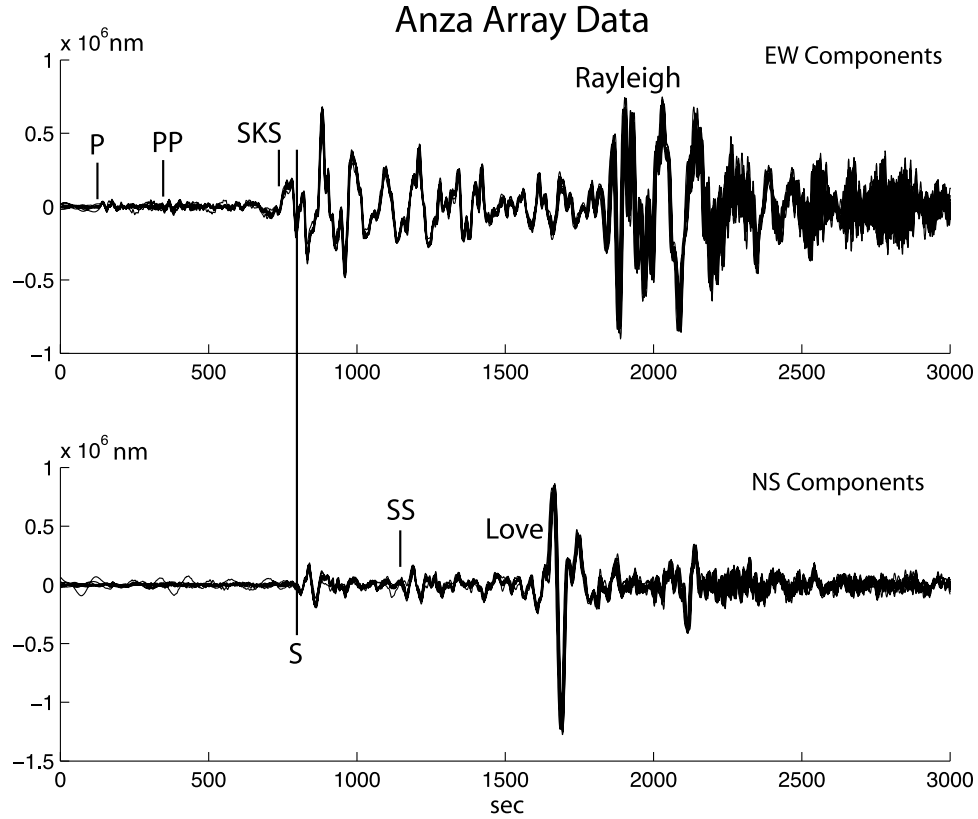


Figure 6. Broadband displacements from the 1 April 2007 $M8.1$ Solomon Islands earthquake recorded on all 10 stations of the network shown in Figure 5. The data have been corrected for instrument response and are plotted on top of each other. Seismic phases for this large teleseism are annotated. Note the remarkable internal consistency of amplitude for this network. The width of the lines, particularly for later arriving phases, indicates the magnitude of the time shifts due to wave propagation across the network.

Form a matrix equation $\mathbf{Gm} = \mathbf{d}$, where

$$\begin{aligned}\mathbf{G} &= \begin{bmatrix} \Delta x_1 & \Delta y_1 \\ \Delta x_2 & \Delta y_2 \\ \vdots & \vdots \\ \Delta x_s & \Delta y_s \end{bmatrix}, \\ \mathbf{m} &= \begin{bmatrix} \frac{\partial u}{\partial x} \Big|_{x_0} \\ \frac{\partial u}{\partial y} \Big|_{y_0} \end{bmatrix}, \\ \mathbf{d} &= \begin{bmatrix} u(x_1, y_1) - u(x_0, y_0) \\ u(x_2, y_2) - u(x_0, y_0) \\ \vdots \\ u(x_s, y_s) - u(x_0, y_0) \end{bmatrix}.\end{aligned}\quad (25)$$

The least squares solution is then found using

$$\mathbf{m} = (\mathbf{G}^T \mathbf{G})^{-1} \mathbf{G}^T \mathbf{d}. \quad (26)$$

This process is repeated assuming each station of the array as a reference station. This is done to examine the stability of the computation since errors in the reference station displacement dominate the data difference matrix, \mathbf{d} .

[25] Figure 7 shows displacement gradients for all 10 stations using this method. Again, the waveforms are remarkably consistent indicating that no individual station has significant amplitude differences from the rest. Even the long-period background noise is consistent on the y derivative traces. Azimuth was computed from the displacement gradient amplitudes using equation (19) for peaks and troughs of the displacement gradient waveforms that exceeded 20% of the maximum amplitude of either component. This was done to reduce the effect of background noise on the azimuth estimates. The rose plots show that the resulting estimates of wave propagation azimuth cluster tightly around 81° and 261° , the theoretical great circle azimuth and back azimuth for waves propagating across the array. This is empirical evidence that the wave gradient analysis can usefully derive fast estimates of wave propagation directions that can then go into further analysis of the radial and transverse motions.

[26] Figure 8 shows an example of detailed wave gradiometry using the vertical components of motion. Data from station FRD have been band-pass filtered between 0.001 and 0.01 Hz. Horizontal wave gradients for the vertical ground motion were computed using the least squares method at station FRD and then applied to find azimuth, wave slowness, geometrical spreading changes, and radiation pattern changes across the array using the results of papers 2 and 3. Basically, we determined the coefficients of

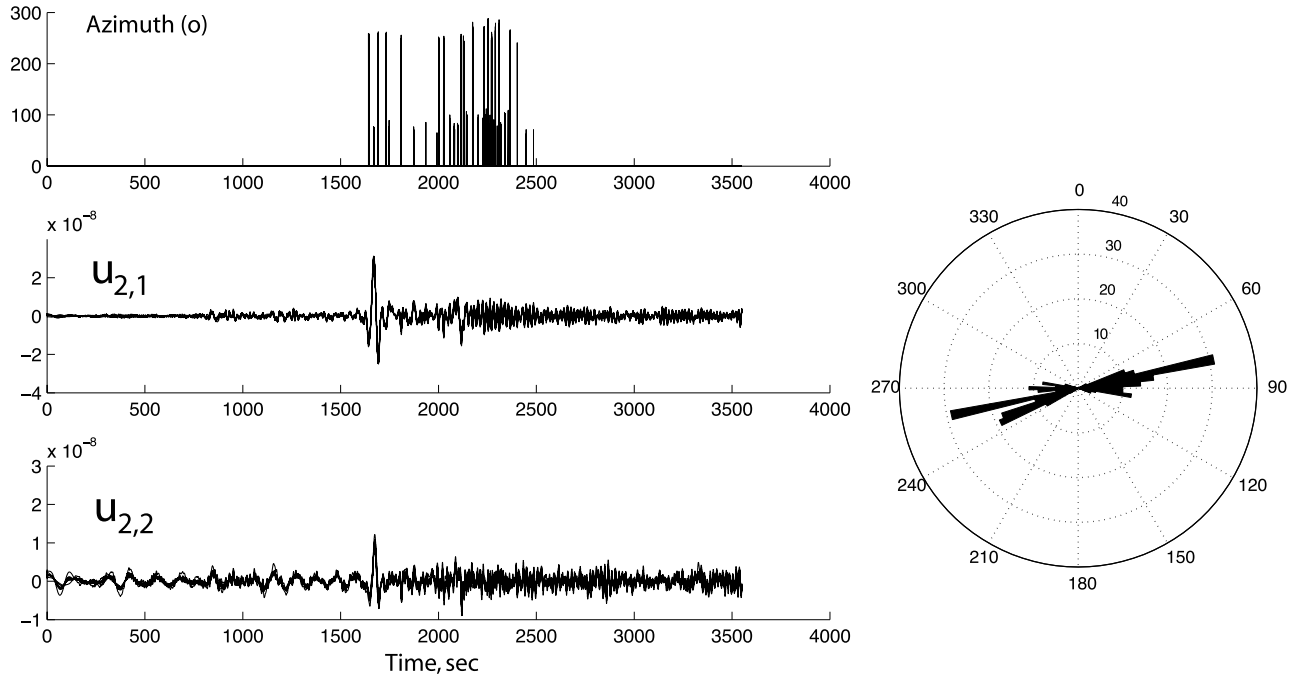
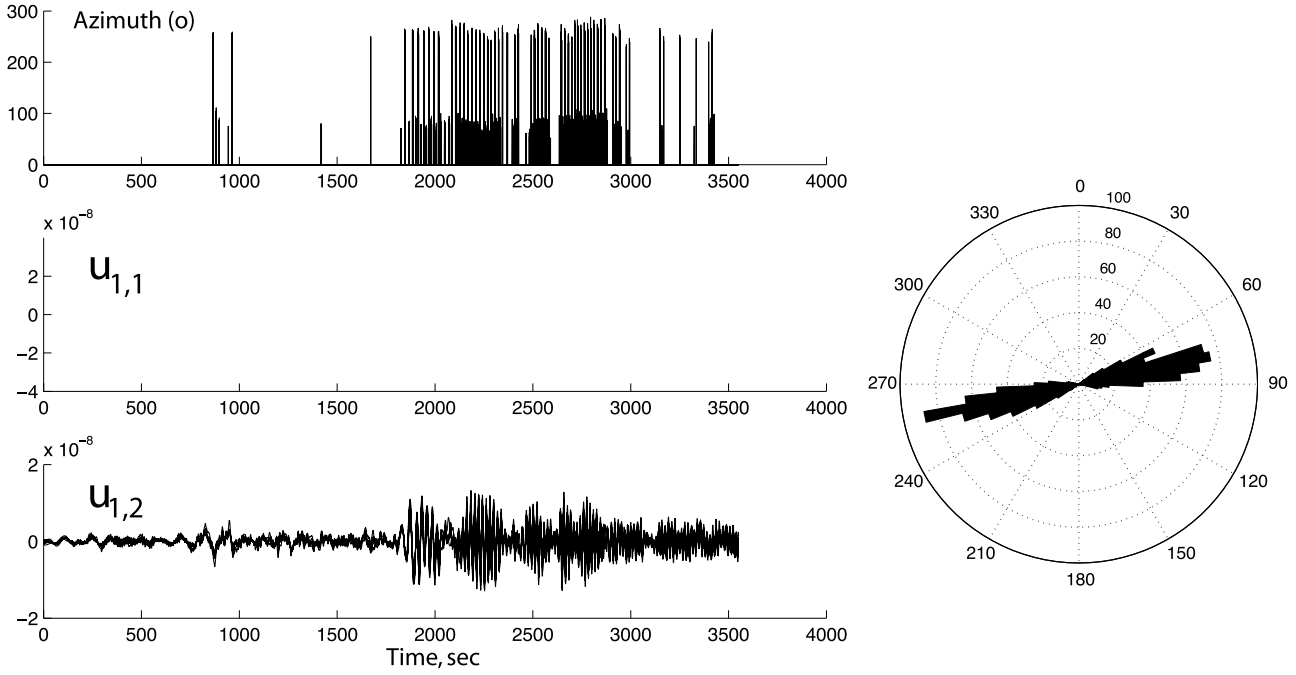


Figure 7. Azimuth analysis of the horizontal displacement gradients computed for the Solomon Islands event. Each plot contains 10 horizontal gradient seismograms. Azimuth is estimated using equation (20) for peaks and troughs that are at least 20% of the maximum amplitude of the horizontal displacement gradients.

equation (13) using the “time domain” method of paper 3. In this method, the instantaneous phases and amplitudes of the analytic signals for the displacement gradient and displacement are computed and the Cartesian wave coefficients found using equations (31) and (32) of paper 3. Azimuth and radial slowness was found from the x and y

slowness (we did not use equation (14)). It was found that the geometrical spreading and radiation pattern parameters were not resolvable but that wave azimuth and slowness were. One of the striking aspects of this computation was the accuracy and ease of seeing the difference between wave directions for waves traveling along the short and long

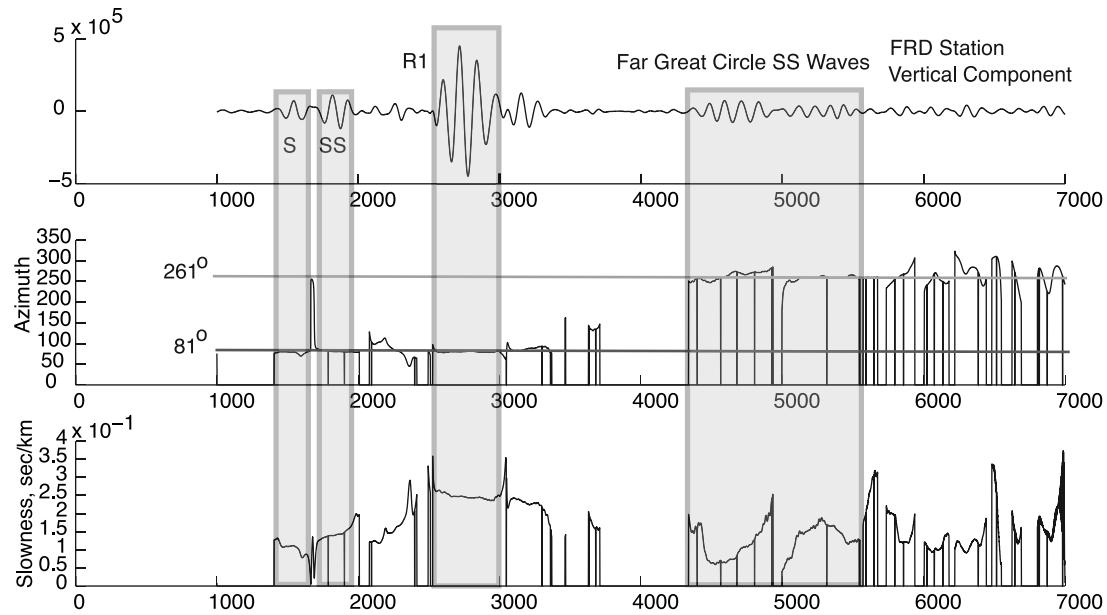


Figure 8. The 2-D gradiometry result using the vertical component of motion and displacement gradients at station FRD. Note that the analysis gives the correct azimuth of propagation for forward and back propagating waves along the great circle. It also gives good estimates of wave slowness for the major seismic phases.

distances of the great circle from the Solomon Islands epicenter. The magnitude and relative differences in wave slownesses for direct S , SS , and $R1$ are also readily apparent. The average observed slowness for S is 0.11 s/km and the expected for this epicentral distance is 0.082 s/km for the IASPEI-91 Earth model. For SS the observed slowness is 0.14 s/km, and the expected slowness is 0.13 s/km. $R1$ shows a range over this frequency band with velocities of 3.7 to 4.0 km/s. Figure 8 also shows artifacts of the method. For example, the “spike” in azimuth between S and SS is a typical effect due to the interference of two distinct seismic phases. The analytic signal method depends on the instantaneous frequency which has occasional discontinuities in it because of the noncausality of the Hilbert transform. However, our preference is to use this method rather than the filter method discussed in paper 2 since the time domain method can be associated more clearly with specific features of the waveform. Please refer to paper 3 for details.

6. Broadband Array and GTSM Strain Fields

[27] The stability and consistency of the displacement gradients computed from the ANZA Seismic Network data suggest that the strains should be equally stable. Figure 9 shows the broadband array strains and the horizontal rotation for all 10 stations of the array. As expected from the previous result, the calculated strains and rotation are virtually identical across the array. Data for the Solomon Islands event recorded at the PBO GTSM stations shown in Figure 5 were obtained and processed using the Java-based Web utility SQUID [Matykiewicz *et al.*, 2007]. The processed data were then filtered with the same band-pass filter as the broadband

array strain data. All PBO strains and the strain computed for station FRD are shown in Figure 10.

[28] The strains at individual PBO stations show considerable variability and are often quite different in waveshape, polarities of major seismic phases, and relative amplitudes. Although seismic phases are quite apparent in the PBO strains, the general inconsistency between strain stations and the broadband array strain is very puzzling. The scatter in the observed strain field no doubt reflects known bore-hole instrument emplacement issues and local ground coupling effects between the strain sensors and surrounding host rock [Hart *et al.*, 1996]. The teleseismic waves recorded by these instruments have wavelengths that are many times larger than the aperture of either array. It is hard to imagine how lateral heterogeneity could produce such large changes in strain well within a single wavelength. The strains computed from the broadband array data (Figure 9) are consistent with the expected smoothing effect of wave propagation in a heterogeneous Earth in that they show little, if any, variation across stations of the array. The PBO strain observations, on the other hand, show the probable effects of heterogeneous coupling of the strainmeters with the local host rock.

7. Discussion

[29] The results of this paper complete the theory needed for basic application of wave gradiometry to three-component seismic wavefields. The assumption of P - SV and SH waves from a point source wave model is a useful starting point for analyzing seismic wavefields recorded by dense arrays of well-calibrated seismometers. Including a radial geometrical spreading function and azimuthal radiation pattern for each wave allows for the potential for inferring

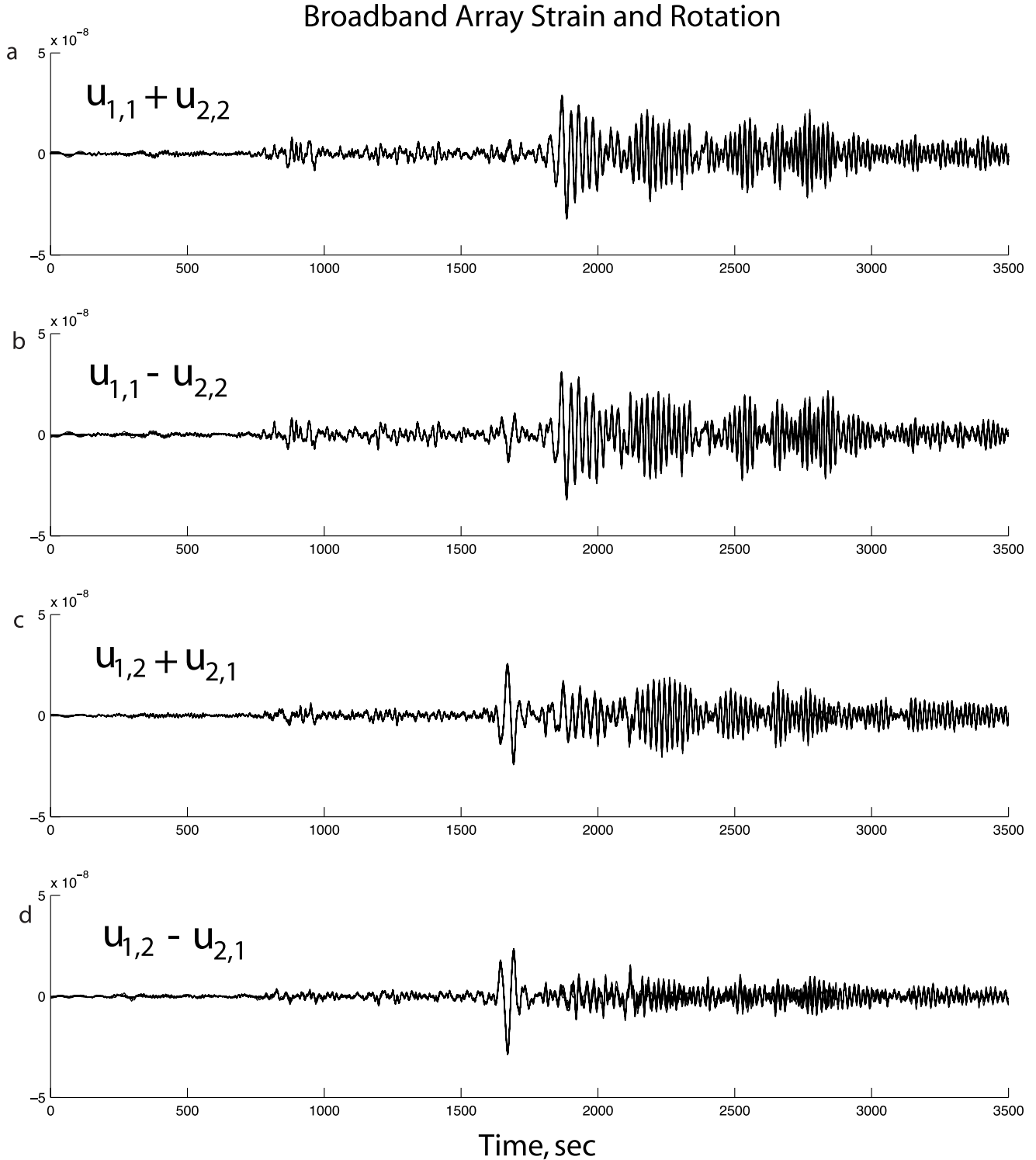


Figure 9. Strain and rotation computed using the horizontal displacement gradients recorded by the ANZA Seismic Network. Each plot shows 10 superimposed seismograms (for each station). The agreement in amplitude and phase is remarkable. (a) The areal strain which should be invariant no matter what Cartesian coordinate system is used to record the data. (b) The differential normal strain. (c) The shear strain. (d) The rotation about the vertical axis.

Earth structure effects in addition to source parameter effects (papers 1 and 2). Because of the nature of the spatial derivatives, source wave propagation effects will probably be more detectable at local or near-regional distances and

might be used to study dynamic rupture on nearby fault surfaces.

[30] Although we have presented an example of a far-field source in this paper in which it should be expected that

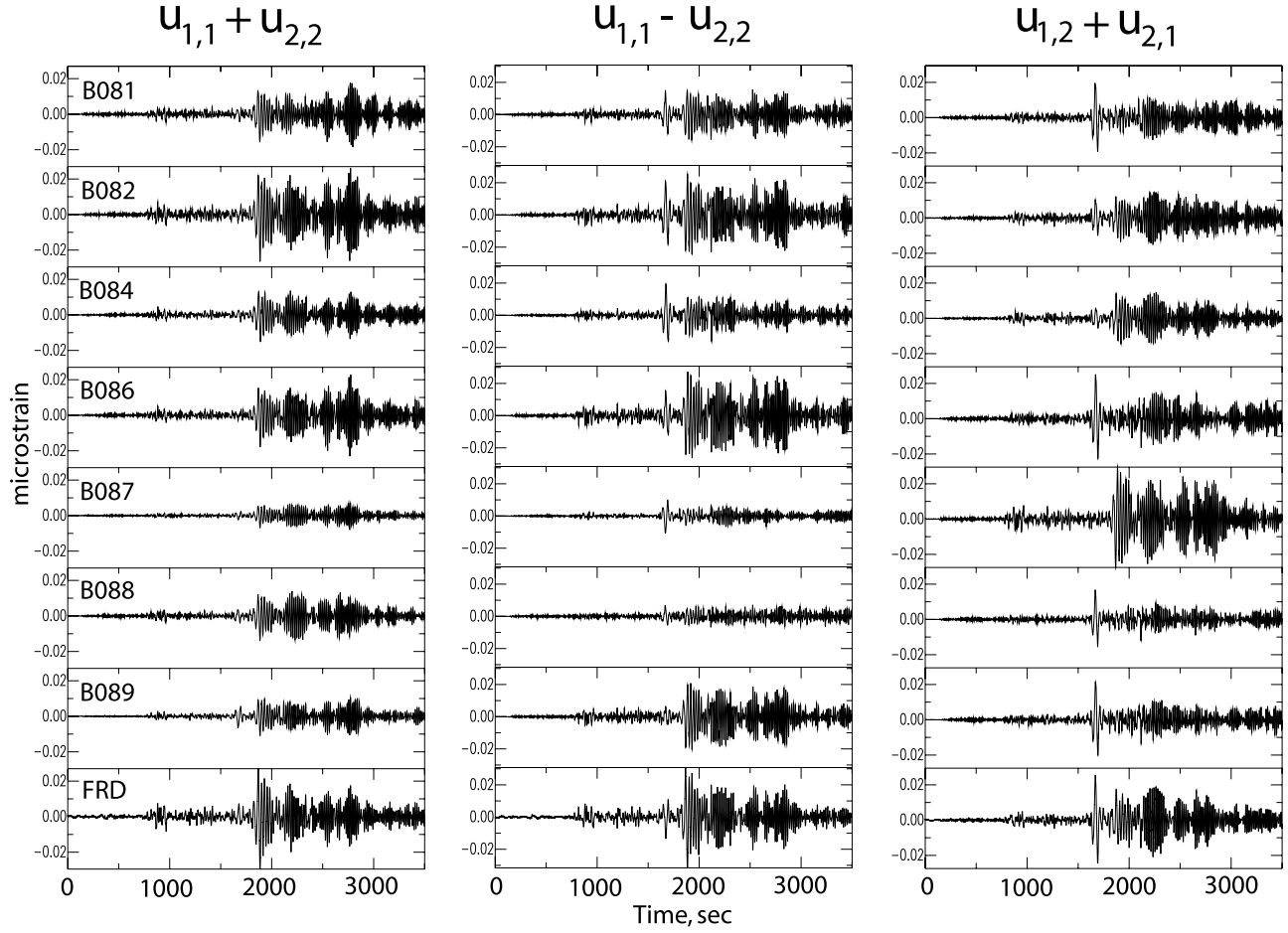


Figure 10. Comparison of strains for station FRD computed using the entire ANZA Seismic Network and strains recorded by the array of PBO GTSM stations. Strains recorded by the GTSM stations are highly variable showing large changes in waveshape and amplitudes. Stations FRD and B087 are collocated as are B082 and B089.

geometrical spreading and radiation pattern effects should not be particularly observable, it is important to emphasize that the theory may find its greatest utility for studying local and regional sources and horizontal variations in structure using nearby controlled sources. The beauty of gradiometry is that it is scale-invariant. Since a seismic array or gradiometer cell needs to be a fraction of a wavelength in dimension, the natural physics of wave propagation virtually guarantees that wave observations will be highly correlated among seismometers. Thus, the usual problems of seismic observations concerning station amplitude and time “statics” should not adversely affect the basic observation or computation of the spatial wave gradient. As for any seismic study, the work will be in interpreting the resulting wave patterns. There are many experiments that can be conceived for testing and using gradiometric techniques. We hoped to demonstrate in this paper that wave gradiometry can link together many existing different data sets and that there is sufficient merit in the technique to use it in standard structure or source studies. The proof of its utility in other experimental designs will be in future, detailed applications.

[31] Using strain to understand seismic waves is a venerable idea that dates back to early research in seismometry

[Benioff, 1935] (see also the short review by Gomberg and Agnew [1996]). However, strain measurements have primarily been used in the geodetic sense for detecting long-duration crustal motions outside of the usual frequency band of modern broadband seismometers [Agnew, 1986; Hart *et al.*, 1996]. Horizontal wave gradients give both strains and rotations that can potentially yield much more information about seismic waves and the effects of Earth structure on those waves. Although there have been about 100 years of experience with the analysis of seismic waves from inertial seismographs, strain and rotation seismometry is only recently starting to yield data sets that can be investigated. Using arrays of seismometers to estimate strains and rotations looks to be a viable way of linking inertial seismometry with differential (strain and rotation) seismometry.

[32] An immediate benefit of this linkage is the calibration of differential sensors. The Anza array result shows that seismic observations from a well-calibrated set of broadband seismometers can produce displacement gradients that are consistent across the array and consistent with what would be expected from wave propagation. Seismic waves with wavelengths many times greater than the array diameter should not show much change even if there is substantial velocity heterogeneity within the array. Unfortunately,

localized strain sensors, like the PBO GTSMs, are subject to localized site conditions and emplacement factors that cannot be predicted. As Figure 10 shows, this leads to significant variability in the measured wavefield that precludes this potentially excellent broadband data set from being used in seismic studies. The results in this paper suggest that the broadband array strains are stable and could be used as a reference strain field to calibrate the GTSMs within the seismic frequency band. This will be pursued in future work.

[33] Well-calibrated installations of inertial, strain, and rotation instruments at a single site or small gradiometer cells made up of a small number of three-component sensors have the potential for being used for analyzing the wavefield in ways that large arrays of inertial seismographs have been used in the past. Wave polarization, slowness, azimuth, and even spatial amplitude changes can be investigated with such point arrays. Making networks and arrays of point arrays should enable the full characterization of the wavefield in a region that can be used to understand both the seismic source and structural heterogeneity. In particular, we speculate that the use of strain and rotation observations could conceivably lead to independent constraints on the effect of localized velocity heterogeneity that could be used in structure inversion studies. Experience with the Anza array shows that gradiometry analyses can be successfully performed with data from some existing networks.

8. Conclusions

[34] Theory for wave gradiometry is developed for horizontal ground motions where P - SV and SH ground motions are mixed. If wave azimuth is a known quantity, the results are identical to previous work on scalar and vertical motions developed in paper 2. Assumption of an azimuthally isotropic point source appropriate for many regional and teleseismic observations yields the new result of a set of simple relations where the tangent of the wave azimuth angle is related to the ratio of the x and y derivatives of any one displacement component. This result coupled with the results of papers 1, 2, and 3 allows the full analysis of polarization and wave parameters using wave gradiometry on three-component seismic data.

[35] Synthetic and observational data are used to show that the simple assumptions of wave gradiometry are effective in analyzing wave trains composed of multiple, diverse wave arrivals. Seismic data from the ANZA Seismic Network in southern California for the 1 April 2007 M8.1 Solomon Islands earthquake show that inferred wave gradients across the network are self-consistent and yield sensible azimuth and slowness values for the observed seismic phases. Strains and rotations computed from the wave gradients are also self-consistent but differ from direct strain observations made by collocated PBO GTSMs within the array. The GTSM data are internally inconsistent and display the effects of local site heterogeneity and installation issues. We suggest that the broadband network strains can be used to calibrate the strainmeters.

[36] Wave gradiometry provides a formalism to link inertial seismic observations with differential (strain and rotation) observations to form a new way of collecting and

analyzing seismic data. Strainmeters are sensitive to the P - SV wavefield through the areal strain, while rotation meters that measure rotation about the vertical axis are sensitive to the SH wavefield. The combination of a three-component broadband sensor, strainmeter, and rotation meter located at a single site can constitute a point seismic array capable of determining wave azimuth, slowness, polarization, and information about geometrical spreading.

[37] **Acknowledgments.** The authors would like to thank Mike Gladwin for his suggestion of looking at the PBO GTSM strain data and to UNAVCO for use of the community “SQUID” software for analyzing raw strain observations. SAC [Goldstein et al., 2003] and GMT [Wessel and Smith, 1998] software packages were used in this work and are acknowledged. Bob Smalley read an initial version of this manuscript and made helpful comments. We would also like to thank David Aldridge for conversations concerning his idea of the point seismic array and two anonymous reviewers for checking the mathematics, suggesting simplifications in notation, and offering other helpful comments. This is CERI contribution 523.

References

- Agnew, D. C. (1986), Strainmeters and tiltmeters, *Rev. Geophys.*, 24, 579–624, doi:10.1029/RG024i003p00579.
- Aldridge, D. F., N. P. Symons, and M. M. Haney (2006), Finite-difference numerical simulation of seismic gradiometry, *Eos Trans. AGU*, 87(52), Fall Meet. Suppl., Abstract S23B-0159.
- Benioff, H. (1935), A linear strain seismograph, *Bull. Seismol. Soc. Am.*, 25, 283–309.
- Bodin, P., et al. (1997), Dynamic deformations of shallow sediments in the Valley of Mexico, part I: Three-dimensional strains and rotations recorded on a seismic array, *Bull. Seismol. Soc. Am.*, 87, 528–539.
- Cochard, A., et al. (2006), Rotational motions in seismology: Theory, observations, simulation, in *Earthquake Source Asymmetry, Structural Media and Rotation Effects*, edited by R. Teisseyre et al., pp. 391–407, Springer, New York.
- Gladwin, M. T. (2007), New options for study of earthquake source parameters and teleseismic arrivals, *Seismol. Res. Lett.*, 78, 266.
- Goldstein, P., D. Dodge, F. Firgo, and L. Minner (2003), SAC2000: Signal processing and analysis tools for seismologists and engineers, in *International Handbook of Earthquake and Engineering Seismology, Part B*, edited by W. Lee et al., pp. 1613–1614, Elsevier, New York.
- Gomberg, J., and D. Agnew (1996), The accuracy of seismic estimates of dynamic strains: An evaluation using strainmeter and seismometer data from Pinon Flat Observatory, California, *Bull. Seismol. Soc. Am.*, 86, 212–220.
- Gomberg, J., et al. (1999), The strain in the array is mainly in the plane (waves below ~ 1 Hz), *Bull. Seismol. Soc. Am.*, 89, 1428–1438.
- Hart, R. H. G., M. T. Gladwin, R. L. Gwyther, D. C. Agnew, and F. K. Wyatt (1996), Tidal calibration of borehole strain meters: Removing the effects of small-scale inhomogeneity, *J. Geophys. Res.*, 101, 25,553–25,571, doi:10.1029/96JB02273.
- Helberger, D. V. (1983), Theory and application of synthetic seismograms, in *Earthquakes: Observations, Theory and Interpretation*, edited by H. Kanamori and E. Boschi, pp. 174–222, North-Holland, Amsterdam.
- Igel, H., U. Schreiber, A. Flaws, B. Schuberth, A. Velikoseltsev, and A. Cochard (2005), Rotational motions induced by the M8.1 Tokachi-oki earthquake, September 25, 2003, *Geophys. Res. Lett.*, 32, L08309, doi:10.1029/2004GL022336.
- Langston, C. A. (2007a), Spatial gradient analysis for linear seismic arrays, *Bull. Seismol. Soc. Am.*, 97, 265–280, doi:10.1785/0120060100.
- Langston, C. A. (2007b), Wave gradiometry in two dimensions, *Bull. Seismol. Soc. Am.*, 97, 401–416, doi:10.1785/0120060138.
- Langston, C. A. (2007c), Wave gradiometry in the time domain, *Bull. Seismol. Soc. Am.*, 97, 926–933, doi:10.1785/0120060152.
- Langston, C. A., A. A. Nyblade, and T. J. Owens (2002), Regional wave propagation in Tanzania, East Africa, *J. Geophys. Res.*, 107(B1), 2003, doi:10.1029/2001JB000167.
- Matykiewicz, J., et al. (2007), SQUID user’s guide version 1.0, 31 pp., UNAVCO, Boulder, Colo.
- Nigbor, R. L. (1994), Six-degree-of-freedom ground-motion measurement, *Bull. Seismol. Soc. Am.*, 84, 1665–1669.
- Roeloffs, E., et al. (2004), Review of borehole strainmeter data collected by the U.S. Geological Survey, 1985–2004, report, 55 pp., EarthScope, Corvallis, Oreg.

- Spudich, P., L. K. Steck, M. Hellweg, J. B. Fletcher, and L. M. Baker (1995), Transient stresses at Parkfield, California, produced by the M7.4 Landers earthquake of June 28, 1992: Observations from the UPSAR dense seismograph array, *J. Geophys. Res.*, 100, 675–690, doi:10.1029/94JB02477.
- Suryanto, W., et al. (2006), First comparison of array-derived rotational ground motions with direct ring laser measurements, *Bull. Seismol. Soc. Am.*, 96, 2059–2071, doi:10.1785/0120060004.
- Takeo, M., and H. M. Ito (1997), What can be learned from rotational motions excited by earthquakes?, *Geophys. J. Int.*, 129, 319–329, doi:10.1111/j.1365-246X.1997.tb01585.x.
- University NAVSTAR Consortium (NAVCO) (2004), Critical design of PBO borehole strainmeter network, 72 pp., Plate Boundary Obs., Boulder, Colo.
- Wessel, P., and W. H. F. Smith (1998), New, improved version of generic mapping tools released, *Eos Trans. AGU*, 79, 579, doi:10.1029/98EO00426.

C. A. Langston and C. Liang, Center for Earthquake Research and Information, University of Memphis, 3876 Central Avenue, Suite 1, Memphis, TN 38152-3050, USA. (clangstn@memphis.edu)